ADVANCED SURFACE PANELING METHOD FOR SUBSONIC AND SUPERSONIC FLOW*

Larry L. Erickson
NASA Ames Research Center

Forrester T. Johnson and F. Edward Ehlers
Boeing Commercial Airplane Co.

SUMMARY

Numerical results illustrating the capabilities of an advanced aerodynamic surface paneling method are presented. The method is applicable to both subsonic and supersonic flow, as represented by linearized potential flow theory. The method is based on linearly varying sources and quadratically varying doublets which are distributed over flat or curved panels. These panels can be applied to the true surface geometry of arbitrarily shaped three-dimensional aerodynamic configurations. The method offers the user a variety of modeling options and is both stable and accurate, the numerical results displaying a marked insensitivity to panel arrangement.

INTRODUCTION

This paper summarizes the general features of an advanced aerodynamic surface paneling method and gives results for both subsonic and supersonic steady flow. The work was originally motivated by limitations in the Woodward-type aerodynamic method used in FLEXSTAB. Although the FLEXSTAB aerodynamic model has several unique capabilities for three-dimensional configurations (e.g., subsonic and supersonic flow, steady and low-frequency unsteady motion (ref. 1)), it also has several faults that are typical of other paneling schemes. For example, results are often sensitive to the manner in which the paneling is laid out, and localized changes in panel density often require corresponding changes to be made over the entire planform. Equally important, the aerodynamic model for fuselage-type components is based on a slender body of revolution plus an interference shell, as shown in figure 1(a). This modeling restriction often results in crude approximations to the geometry of aircraft, especially fighter-type aircraft.

The goal of this development work is to produce a reliable subsonic/supersonic panel method that accurately represents the actual surface geometry of realistic aircraft as shown in figure 1(b). To produce such a method

*This work was performed under contract NAS2-7729 for NASA Ames Research Center.

requires flat and curved panels that can be arbitrarily oriented in space (e.g., panels should incline toward the flow direction and panel side edges should not have to be parallel to the flow). To be usable and reliable, the method must produce accurate results that are not sensitive to the size, shape, and arrangement of the paneling; in turn, this capability makes automated paneling practical. In addition, the method must be efficient. The results indicate that these requirements can be met for both subsonic and supersonic analysis problems (specify shape, solve for pressure) and for subsonic design problems (specify pressure, solve for shape).

SYMBOLS

Values are given in SI units. The calculations were made in U.S. customary units.

A_{ij}	influence coefficient matrix relating singularity strength parameters to perturbation velocities, m^{-1}
b	wing span, m
$[C]$	matrix relating doublet strength coefficients and doublet singularity parameters
C_L	lift coefficient
C_{L_α}	lift curve slope
C_m	pitching moment coefficient
$C_p = \frac{p - p_\infty}{q_\infty}$	pressure coefficient
$\Delta C_p = C_{p_\ell} - C_{p_u}$	
c	local chord
c_ℓ	section lift coefficient
K	kernel function in equation (4), m^{-2}
k	panel number
L	body length, m
M	Mach number
N	number of singularity parameters associated with panel K; also, number of chordwise and streamwise panels in figure 5.

N_o	aerodynamic center location as fraction of local chord
$\vec{n}$	unit normal to aerodynamic surface
P_j	the set of N points corresponding to the μ_j in equation (2)
p	pressure, N/m^2
q	dynamic pressure, N/m^2
R	see equation (3)
r	body radius, m
S_k	area of integration over panel k, m^2
$\vec{U}_\infty$	free-stream velocity vector, m/sec
$U_\infty = \lvert\vec{U}_\infty\rvert$	
$\vec{V}$	total velocity vector, m/sec
$\vec{v}^k_{i(j)}$	perturbation velocity vector at field point i due to the N singularity parameters μ_j associated with panel k, m/sec
W_j	weighting values used in equation (3)
x,y	coordinates in chordwise and spanwise directions, respectively, m
α	angle of attack, degrees or radians
Γ	bound circulation
$\mu(\xi,\eta)$	doublet strength distribution, m^2/sec
μ_j	doublet singularity parameter, m^2/sec
$\mu_o, \ldots \mu_{\eta\eta}$	coefficients in the expression for $\mu(\xi,\eta)$
ξ,η,ζ	local orthogonal coordinate axes associated with individual panels, m
ϕ	perturbation potential, m^2/sec; also, circumferential angle in figures 15 and 16
ρ	fluid density, kg/m^3
$\sigma(\xi,\eta)$	source strength distribution, m/sec

Subscripts:

i	field point
j	singularity parameter or singularity parameter point
ℓ	lower surface
u	upper surface
∞	free-stream value

Operator:

$\vec{\nabla}$	gradient (with respect to field point coordinates), m^{-1}

GENERAL FEATURES OF THE METHOD

The approach is fundamentally the same for both subsonic and supersonic flow. (More specific details of the mathematics are given in refs. 2 and 3.) As in several other methods, it is based on the singular source and doublet solutions to the linearized subsonic and supersonic potential flow equations. The primary differences in the present method are (1) the use of higher order forms for the spatial distribution of these singularity strengths, and (2) the retention of curvature effects for the panels on which these singularities are distributed. Specifically, the sources are assumed to have a linear strength distribution and the doublets have a quadratic strength distribution over the panels. (Both triangular and quadrilateral panels are allowed.) The panels can be used for both actual surface paneling, or for mean surface paneling as indicated in figure 1(b). Velocity or mass flux (ref. 3) type boundary conditions can be imposed on either the mean or actual surface boundary; alternately, potential-type boundary conditions can be imposed on the interior of closed bodies. These alternatives are sketched in figure 2, and are illustrated by later examples. Initial results indicate the modeling technique of figure 2(b) is generally the best choice for closed bodies — it gives accurate results and requires considerably fewer calculations than velocity-type boundary conditions.

For both subsonic and supersonic flow, the integrations giving the panel influence coefficients have been obtained in closed form. This has the following advantages over a numerical integration form:

1. The influence coefficients can generally be computed faster and more accurately. This is especially true for regions in which the integral is singular.

2. The coding is much simpler, especially for nonstreamwise side edges. In the supersonic case, all Mach cone/panel intersections are automatically treated.

CHARACTER OF THE NUMERICAL MODELS

Networks

For user convenience, the numerical model is cast in the form of panel networks. These networks are a collection of either source or doublet panels and are independently defined over various portions of the aircraft surface as illustrated in figure 3.

Associated with each network are discrete sets of standard points. As described later, some points are used for expressing the source and doublet singularity strength distributions in terms of singularity parameters whose values are to be determined. An equal number of points are used as control points. Control points located at panel centers are used to impose local boundary conditions expressed in terms of either velocity or velocity potential. Additional control points along network edges are used to match the flow properties along common edges of adjacent networks.

The edge control points are also used to impose auxiliary conditions such as the Kutta condition at subsonic trailing edges and for the design case to ensure the proper closure of surfaces (e.g., to specify trailing edge thickness).

Four basic network types are used: source/analysis, doublet/analysis, source/design and doublet/design. In addition, variations of these four types are used for special purposes such as wake paneling. The features that distinguish one network type (and variations thereof) from another are the number and location of the singularity parameter points and the control points (ref. 2, appendices B and C). Particular combinations of singularity parameter points and control points are selected for their ability to produce stable numerical results for the boundary value problem under consideration.

To apply the method, the user must represent the aircraft surface (and the wake for subsonic flow) as a collection of paneled networks, and specify the network type(s) and appropriate boundary conditions. For each network, the code then sets up all the proper singularity parameter and control point locations.

Singularity Strength and Singularity Parameters

A brief description of the singularity strength definition for both source and doublet networks is given in reference 2. An expanded explanation is given here for the specific case of a doublet/analysis network.

Figure 4(a) shows a network comprised of 25 panels. (The surface shape of these panels is obtained by least square fitting a paraboloid to corner points of neighboring panels (ref. 2). Also shown are the locations of the 49 singularity parameter points; one point is at the center of each panel and the

other points are distributed along the network edges. For this particular network, the control points are arranged in a nearly identical fashion.[1]

Associated with each panel k of the network is a six-degree-of-freedom quadratic-doublet strength distribution of the form

$$\mu^k(\xi,\eta) = \mu_o{}^k + \mu_\xi{}^k \xi + \mu_\eta{}^k \eta + \frac{1}{2} \mu^k_{\xi\xi} \xi^2 + \mu^k_{\xi\eta} \xi\eta + \frac{1}{2} \mu^k_{\eta\eta} \eta^2 \qquad (1)^2$$

In equation (1), ξ and η are local orthogonal coordinates that lie in a reference plane associated with panel k, as illustrated in figure 4(b). (This plane is tangent to the curved panel at the panel center and is nearly parallel to the plane passing through the midpoints of the line segments connecting the corner points of the curved panel.) For each panel, the six coefficients in equation (1) are expressed in terms of selected subsets of the network singularity parameters. For panel k, this subset consists of N singularity parameters μ_j that are associated with panel k and with the panels directly adjacent to panel k.[3] For convenience, the N points at which these singularity parameters are defined are designated P_j. In equation form,

$$\begin{Bmatrix} \mu_o{}^k \\ \mu_\xi{}^k \\ \mu_\eta{}^k \\ \mu^k_{\xi\xi} \\ \mu^k_{\xi\eta} \\ \mu^k_{\eta\eta} \end{Bmatrix} = \underset{6\times N}{[C]}_k \underset{N\times 1}{\{\mu_j\}_k} \qquad (2)$$

Thus, for panel 13 of figure 4(a), $k = 13$, $N = 9$, and $j = (17\text{-}19, 24\text{-}26, 31\text{-}33)$.

The linear relationship given by equation (2) is determined by the method of weighted least squares. That is, for each panel k, the expression

$$R^k = \frac{1}{2} \sum_j W_j [\mu^k(\xi_j,\eta_j) - \mu_j]^2 \qquad (3)$$

---

[1]The only difference is that the edge control points are inset slightly from the network edge; this is done to prevent the influence coefficients from becoming infinite.

[2]The symbol k is a superscript, not an exponent.

[3]Only these neighboring points are used in order to localize any irregularities that may appear in the total solution.

is minimized with respect to the six coefficients appearing in $\mu^k(\xi_j,\eta_j)$. The summation in equation (3) ranges over the points P_j. The weight W_k is given a much larger value than the weights $W_{j\neq k}$. This forces the least squares fit of equation (1) (to the N singularity parameters at points P_j) to be best at panel k. This is illustrated in figure 4(c) for k = 13. (In practice $W_k = 10^8$ and $W_{j\neq k} = 1$ are used.)

Note that the sole reason for the above least squares procedure is to express the assumed panel doublet strength distribution in terms of a neighboring subset of the unknown singularity parameters. This procedure is required because the higher order form for $\mu^k(\xi,\eta)$ given by equation (1) associates more than one coefficient with a single panel. If a constant strength distribution were chosen, that is, $\mu^k(\xi,\eta) = \mu_o{}^k$, then there would be only one coefficient per panel. Consequently, the coefficients $\mu_o{}^k$ themselves could be taken as the basic unknowns. (In fact, this is the concept employed by the Woodward constant pressure panels.)

Because of the least squares formulation, the singularity strength $\mu^k(\xi,\eta)$ of a panel is defined beyond the panel boundary. For the purpose of computing influence coefficients, however, the range of ξ and η is confined to the panel interior and boundary. This range is illustrated in figure 4(c) by the solid portion of the curve for $\mu^{13}(\xi,\eta)$.

Note that the doublet singularity strengths of adjacent panels are not forced to be continuous at the panel edges. For sufficiently dense paneling, however, the strengths are nearly continuous. Thus, the appearance of doublet strength mismatches at panel edges provides a valuable indicator of locally inadequate paneling. (This is illustrated below by the results for the randomly paneled swept wing.)

Influence Coefficients and Determination of the Singularity Parameters

Having each of the panel singularity strength distributions expressed in terms of the unknown singularity parameters enables the perturbation potentials and velocities to be computed in terms of these parameters. Imposing boundary conditions then yields a set of influence coefficient equations from which the singularity parameters can be computed. The discussion below illustrates this for boundary conditions expressed in terms of velocity.

The symbol $\vec{v}^k_{i,(j)}$ is used to denote the perturbation velocity at field point i due to panel k; the subscript (j) indicates that the velocity depends on several singularity parameters μ_j (at points P_j). This velocity is computed from the doublet singularity strength $\mu^k(\xi,\eta)$ and the doublet velocity potential $K(\xi_i - \xi, \eta_i - \eta)$ by an integral of the form (ref. 4, p. 166)

$$\vec{v}^k_{i(j)} = \iint_{S_k} \mu^k(\xi,\eta)\, \vec{\nabla} K(\xi_i - \xi, \eta_i - \eta)\, d\xi\, d\eta \qquad (4)$$

where (ξ_i, η_i) is the field point i, and the gradient operator is taken with respect to the field point coordinates (i.e., $\partial/\partial\xi_i$, etc.). The expression for the velocity kernel K differs for subsonic and supersonic flow, as does the region of integration S_k. For subsonic flow, S_k is the entire panel area. For supersonic flow, S_k is that portion of the panel that lies in the upstream Mach cone emanating from the field point.

The result of the integration in equation (4) is that the right-hand side of the equation becomes a linear algebraic equation in the network singularity parameters μ_j.[4] For the single network of figure 4(a), the total velocity at any control point i, due to all the panels, is given by

$$\vec{V}_i = \vec{U}_\infty + \sum_{k=1}^{k=25} \vec{v}^k_{i(j)} = \vec{V}_i(\mu_j) \tag{5}$$

where $\vec{U}_\infty$ is the free-stream velocity vector. Imposing the boundary condition $\vec{V}_i \cdot \vec{n}_i = 0$, where $\vec{n}_i$ is the unit normal vector at control point i, gives

$$\sum_{k=1}^{25} \vec{v}^k_{i(j)} \cdot \vec{n}_i = -\vec{U}_\infty \cdot \vec{n}_i \qquad i = 1, \ldots 49$$

When cast in matrix form, this equation becomes

$$\underset{49\times49}{\left[A_{ij}\right]} \begin{Bmatrix} \mu_1 \\ \cdot \\ \cdot \\ \cdot \\ \mu_{49} \end{Bmatrix} = - \begin{Bmatrix} \vec{U}_\infty \cdot \vec{n}_1 \\ \cdot \\ \cdot \\ \cdot \\ \vec{U}_\infty \cdot \vec{n}_{49} \end{Bmatrix} \tag{6}$$

Each row i of the influence coefficient matrix A_{ij} represents a boundary condition imposed at one of the 49 control points. Each column j corresponds to one of the 49 singularity parameters μ_j. The matrix A_{ij} is constructed one row (control point) at a time. For each row, one cycles through the panels and enters the contributions of each panel to the appropriate columns of A_{ij}. For example, panel 13 of figure 4(a) would contribute a value to columns 17-19, 24-26, and 31-33. (Other panels would also contribute values to some of these same columns, and these values would be added to those from panel 13.)

For more than a single network, the procedure is exactly the same except that the matrices in equation (6) expand in size so as to incorporate all the panels, all the singularity parameters, and all the control points of every network. (At this point the networks effectively lose their distinct identities.) The general form of equation (6) is then

---

[4]This integration, and a similar one for the linear source distribution, has been carried out analytically for both subsonic and supersonic flows. See references 2 and 3, respectively.

$$\underset{M\times M}{[A]}\ \underset{M\times 1}{\{\mu\}} = \underset{M\times 1}{\{b\}} \tag{7}$$

where M is the total number of singularity parameters (and control points) for all the networks. Hence $\{\mu\}$ can be solved for, and then the velocities can be calculated from $\vec{V}_i(\mu_j)$ as indicated by equation (5). (The value $k = 25$ appearing in equation (5) would be replaced with the total number of panels in all the networks.) Knowing the velocities, the pressures can then be calculated from appropriate velocity-pressure relationships.

RESULTS AND DISCUSSION

The following numerical results are presented to illustrate the various capabilities of the method.

Subsonic Flow[5]

Localized panel density changes.- Figure 5 shows the right half of an aspect-ratio-two wing modeled as three doublet/analysis mean surface networks and two wake networks. The panel density in wing networks I and II is held fixed while the panels in wing network IV vary from 4 to 144, with corresponding changes made to the trailing wake network (number V). The lift curve slope and chordwise center of pressure location N_o are only slightly affected by this large change in local panel density. Another feature illustrated by this example is that panel edges from adjacent networks are not required to be aligned. For $N = 4$ in fact, none of the panel edges internal to network IV are aligned with those from networks I and II.

When this set of cases was first run it was expected that only cases $N = 2$ and $N = 6$ would be successful because these are the only arrangements in which network IV has edge control points directly opposite those of networks I and II. It was somewhat surprising to discover how forgiving the numerics actually are to such network mismatches.

Convergence behavior.- The aspect-ratio-two wing was also used to study solution convergence behavior. In this case, single doublet/analysis networks were used for the wing. One network used uniform panel spacing and the other used cosine spacing, as shown in figure 6(a). The variation in lift coefficient with number of panels is shown in figure 6(b), along with the highly accurate and converged solution of Rowe (ref. 6). The convergent character of the panel solutions is clearly seen. The cosine spacing probably converges faster than the uniform spacing because of the greater panel density at the wing leading edge and tip where pressure gradients are largest. Chordwise variations in $\Delta C_p = C_{p_\ell} - C_{p_\mu}$ at $y/(b/2) = 0.5$ are shown in figures 6(c)

---

[5]All the cases shown are for incompressible flow. The method is easily extended to compressible flow by stretching the aircraft geometry in the streamwise direction by the Prandtl-Glauert rule (ref. 5, p. 84).

and 6(d) for the cosine and uniform spacing cases, respectively, along with results from reference 6. Again, cosine spacing gives more accurate results than uniform spacing for a given number of panels.

Insensitivity to panel arrangement.- Figure 7 illustrates the insensitivity of the method to extremes in panel size, shape and arrangement. A swept wing has been paneled in a regular and in a random fashion, and the vortex spline method of reference 7 was used to calculate results for the regular paneling. A doublet/analysis network of the present method was used for the random paneling. The spanwise lift distributions computed by the two methods are nearly identical as seen in figure 7(b). Chordwise pressure distributions at $y/(b/2) = 0$ are plotted in figure 7(c). Here, the results of the present method differ from those of the reference solution towards the leading edge where the pressure gradient becomes large. Note that the pressures predicted by the present method are actually discontinuous at panel edges. When the panel density is sufficiently fine, these discontinuities essentially vanish. The large mismatches are an indication of locally inadequate panel density over the forward portion of the wing. This agrees with figure 7(a), where it is seen that only two panels are used between the leading edge and about the 30% chord line.

The above examples of random paneling and of localized panel density changes (fig. 5) demonstrate the extreme forgiveness of the method to irregular paneling, a feature that greatly enhances its practical usability for applications involving complex geometries where regular, evenly spaced paneling cannot always be constructed.

Alternative surface paneling models.- The preceding examples of lifting surfaces are all mean surface models. In figure 8, results are presented for three different upper and lower surface paneling models of an aspect-ratio-two, 12% thick rectangular wing.

The first model was somewhat similar to that of the reference solution and employed a source/analysis network on the wing surface combined with a doublet/analysis network lifting system on the camber surface. Zero normal velocity was prescribed at control points of both networks. The second model used a doublet/analysis network on the wing surface with zero total potential specified on the interior side of the surface. For this formulation it was necessary to close the wing by paneling the tip. The third model (pioneered by Morino (ref. 8) employed superimposed source/analysis and doublet/analysis networks on the wing surface. Zero perturbation potential was specified on the interior side of the wing surface and the source strengths were set equal to the negative of the normal component of free-stream velocity (see fig. 2(b). This model appeared to be somewhat more forgiving than the previous model regarding closed surfaces and it was unnecessary to panel the tip.

The last two models have certain advantages over the first. The influence coefficients require the computation of a scalar ϕ rather than a vector $\vec{\nabla}\phi$; moreover, the scalar is a lower order expression, which is cheaper to compute. The influence coefficients need not be saved for postprocessing since surface velocities can be calculated directly from doublet strength gradient. This fact also implies that velocities may be calculated everywhere on the

surface, not just at control points, which, in turn, allows more accurate calculation of forces. Note that the use of superimposed source and doublet networks in the third model is only modestly more expensive than the use of a doublet network alone since source strength is prescribed and terms common to both the source and doublet influence coefficients need be computed only once.

Efficiency of analysis networks.- Figure 9 is an illustration of wing body surface paneling with results computed from the present method and from the method of reference 9. Figure 9(a) shows the surface paneling used by the present method. A total of 160 curved, linear-strength source/analysis panels were used for the half airplane, 96 on the body and 64 on the upper and lower wing surfaces. An additional 32 doublet/analysis panels were placed on the wing camber surface and 13 wake panels were also used (some of which extended the wing doublet panels to the centerline, i.e., $y = 0$).

Results from the method of reference 9 were obtained using 936 flat, constant-strength source panels and 12 lifting elements. This is typical of the number of panels required by this method for wing-body applications.

Upper and lower wing surface pressures predicted by the two methods are shown in figure 9(b) for two span stations. The agreement is excellent at $y/(b/2) = 0.68$ and at two additional inboard stations which are not shown. The discrepancy at $y/(b/2) = 0.90$ is possibly due to the fact that the method of reference 9 underestimates spanwise velocities near wing tips, and may also be partly caused by the large width used for the outboard panels in the present method. The table in figure 9 shows that the lift and pitching moment coefficients are also in close agreement.

The table in figure 9 also gives the CPU times for the two methods. The present method enjoys a better than 20-to-1 advantage over the method of reference 9 due to the large reduction in the number of panels required.

Even on a panel-by-panel basis, the higher order singularity panels of the present method are competitive with the constant strength panels of reference 9. Figure 10 gives an estimate of CPU time comparisons between the pilot code of the present method and the highly optimized TEA230 program of reference 9. The CPU time represents time for setting up panel geometry, singularity strength and control point quantities, calculation of influence coefficients, and equation solving. The range of CPU times for a given number of panels reflects differences between sources and doublets and between near-field and far-field calculation times.

Wing design in presence of fixed fuselage geometry.- Figure 11 illustrates the three-dimensional design capability of the method.[6] This example shows how design-type panel networks are able to reproduce an original geometry from a modified geometry, using the pressure distribution of the original geometry as boundary conditions.[7] The pressure distributions

[6]Another application of the design networks is given in reference 10, which treats separated leading edge vortex flow.

[7]In an actual application, the desired geometry corresponding to a specified pressure distribution would of course not be known a priori.

calculated from the original geometry are shown by the solid curves in figure 11(b). A modified geometry and the corresponding pressures are shown by the dashed curves in figures 11(c) and 11(b), respectively. By replacing the analysis network in the modified geometry region with a design network, the desired geometry corresponding to the specified pressure distribution was then computed. After two iterations, the designed geometry and corresponding pressures are nearly identical to the originals, as shown by the circles in figures 11(b) and 11(c).

Supersonic Flow

Flow over spindles.- Figures 12 through 16 show results for flow over axisymmetric spindles and illustrate several features of the linear source panels.

Figure 12 shows a 0.1 fineness ratio spindle with a random paneling arrangement. Because of this extreme panel layout, and the use of only flat panels, the resultant surface is somewhat distorted. For example, surface indentations can be seen in the front view. Even so, the predicted pressures at panel control points, given by the dots in figure 12, are in remarkably good agreement with the exact method of characteristics solution.

Figure 13 is for the same spindle as in figure 12 but the paneling is laid out in a regular fashion. This paneling was used to compute source panel solutions for both a constant strength and the linearly varying strength distribution of the present method. These solutions are shown in figure 13, along with an axisymmetric line source solution. For this particular configuration, the results from all three methods are in good agreement with the exact solution.

Figure 14 is for the same configuration as figure 13, except that the fineness ratio has been halved. In this case the present linear source panels and the axisymmetric line source give the same results, but the constant-strength source panels show considerable differences, indicating a loss of accuracy.

Another indication that the linear source panels are more reliable than constant strength panels is provided by figures 15 and 16. Here, the 0.05 fineness ratio spindle of figure 14 is at $\alpha = 5°$ and pressures are given at three circumferential angles. Figure 15 is for constant-strength source panels, while figure 16 is for the linearly varying source panels of the present method (both cases are for the paneling shown in figure 13). The oscillations that occur in the constant-strength source panel solution are a clear indication of numerical stability problems. Note that the linear source panel solutions do not exhibit this oscillatory behavior.

Wing with subsonic and supersonic leading edges.- Figure 17 shows results for a wing having both a subsonic and a supersonic leading edge. Results predicted by a single network of planar doublet/analysis panels are in good agreement with the exact linearized theory solution in reference 11. By using two networks, with the special Mach line on the left as a network boundary,

the discontinuity in pressure at the Mach line can be represented even more accurately. For this case (not shown), the pressure remains exactly constant in the region between the supersonic leading edge and the special Mach line.

It should also be noted that the present method does not require artificial "diaphragm" panels between the subsonic leading edge and the right-hand side special Mach line.

Upper and lower surface paneling of thin wing.- Figure 18 shows the upper and lower surface paneling used on a 3% thick arrow wing (wing number 2 of refs. 12 and 13). This is a particularly severe test of the method due to the presence of internal waves, which for a source-paneled wing can repeatedly reflect from the closely spaced upper and lower wing surfaces with increasing intensity. To suppress these internal waves, separate source and doublet networks having identical paneling were superimposed, that is, each panel shown in figure 18 represents both a source and a superimposed doublet. Boundary conditions of the type shown in figure 2(b) were employed so that the modeling was the same as for the third model of the $\mathcal{A}R = 2$, 12%-thick rectangular wing of figure 8.

Predicted and experimental upper and lower surface pressure distributions are shown in figure 19 for four spanwise stations. The predicted pressure distribution is smooth and compares well with the experimental data except in the tip region. The oscillations at the tip are thought to be caused by the combined effect of the discontinuous doublet strength (at panel edges) and the special Mach line emanating inboard from the leading edge of the wing tip. The discontinuity in doublet strength is equivalent to a concentrated line vortex, which produces infinite singularities propagating along Mach cones. This is perhaps causing the oscillations in the predicted wing tip flow field. It is anticipated that this problem will be overcome by the implementation of a new doublet network currently under development. This doublet network achieves exact continuity of doublet strength across panel edges by splitting each (quadrilateral) panel into four triangles via the panel diagonals. A different quadratic doublet distribution is defined on each triangle with the provision that doublet strength and gradient must be continuous across triangle edges within the panel. This leads to a doublet distribution on each quadrilateral panel with eight degrees of freedom versus the original six — enough to produce continuity of doublet strength (and in most cases gradient) across panel edges. Such a formulation would seemingly increase the number of influence coefficient computations for each panel by a factor of 3 (the increase in the number of edges). In fact this is not the case because the enhanced continuity properties of the new doublet distribution allow one to neglect terms that would cancel analytically. (With the present network, the lack of strict continuity requires the terms to be retained.) Such terms account for approximately 70% of the influence coefficient operation count.

Also, a more efficient version of the two separate but superimposed source and doublet panel networks is being developed. This will result in a single "composite" panel network for which certain terms in the influence coefficients will only have to be computed once, instead of twice as is done in the superimposed case.

Forebody pressures on B-1.- Figure 20 shows the paneling used on the forebody section of the B-1 bomber. The modeling technique was the same as in the preceding example. Pressure coefficient results at $M = 1.6$ are shown in figure 21 along the upper and lower fuselage lines. Also shown are the experimental data and finite difference results reported in reference 14. The panel method results are in good agreement along the lower fuselage line and along the upper fuselage line up to the canopy region. In the region aft of the canopy, the comparison is poorer; this again may be due to the discontinuity in doublet strength across panel edges discussed in the previous example.

The CPU time for the finite difference calculations on the forebody took about 55 min on a CDC 7600 (ref. 14). The panel method results took about 1 min, also on a CDC 7600.

Superinclined panel.- The current source and doublet panels must be inclined at angles less than that of the Mach cone. Currently under development is a "superinclined" panel that can be inclined ahead of the Mach angle. With this capability it will be possible to place panels at nacelle inlets and exhausts for:

1. closing the nacelle volume so that potential-type boundary conditions can be specified in the interior.

2. sealing off inlets to prevent the propagation of waves into the interior (which can degrade numerical accuracy).

3. specifying exhaust mass flows.

These features are illustrated in figure 22.

The superinclined panels represent an initial value problem type of behavior and require two boundary conditions on the downstream panel side. Although these panels look like blunt surfaces, they do not influence the upstream flow.

CONCLUDING REMARKS

A higher order panel method for linearized subsonic and supersonic flow has been described. Numerical results illustrate the following features:

1. The paneling can be applied to the true surface geometry of arbitrarily shaped aerodynamic configurations.

2. Both supersonic and subsonic analysis, and subsonic design problems can be solved. In the design mode, the geometry required to produce a specified pressure distribution is determined. One or more components of a configuration can be designed in the presence of other components whose geometrical shapes are fixed.

3. The method offers the user a variety of modeling options. For example, with wing-like components, all the usual thin surface approximations are available. For more accurate results, the paneling and boundary conditions can be applied to the wing upper and lower surfaces. For closed bodies, either velocity or potential-type boundary conditions can be imposed.

4. For subsonic flow, the method is both stable and accurate. Unlike many other methods, the numerical results display a marked insensitivity to the size, shape, and arrangement of panels. Good accuracy is obtained with relatively sparse panel densities; convergence to highly accurate results occurs at moderate panel densities. For supersonic flow, spurious oscillations in pressure sometimes occur. It is anticipated that this problem can be solved by eliminating the discontinuity in doublet strength at panel edges.

5. The method is efficient. Individual panel influence coefficient calculation times are competitive with existing body surface paneling methods that use lower order singularities, and overall matrix sizes are much smaller because of the reduced number of panels required. In addition, the influence coefficient integrals are all evaluated in closed form.

REFERENCES

1. Perkin, B. R.; and Erickson, L. L.: FLEXSTAB — A Computer Program for the Prediction of Loads and Stability and Control of Flexible Aircraft. Proceedings of the SCAR Conference, NASA CP-001, 1977. (Paper no. 12 of this compilation.)

2. Johnson, F. T.; and Rubbert, P. E.: Advanced Panel-Type Influence Coefficient Methods Applied to Subsonic Flows. AIAA Paper 75-50, Jan. 1975.

3. Ehlers, F. E.; Johnson, F. T.; and Rubbert, P. E.: A Higher Order Panel Method for Linearized Supersonic Flow. AIAA Paper 76-381, July 1976.

4. Kellog, O. D.: Foundations of Potential Theory, Dover Publishing Co., 1953.

5. Ashley, H.: Engineering Analysis of Flight Vehicles. Addison-Wesley Publishing Co., 1974.

6. Rowe, W. S.: Collocation Method for Calculating the Aerodynamic Pressure Distributions on a Lifting Surface Oscillating in Subsonic Compressible Flow. AIAA Symposium on Structural Dynamics and Aeroelasticity, Boston, Mass., Aug. 1965.

7. Mercer, J. E.; Weber, J. A.; and Lesferd, E. P.: Aerodynamic Influence Coefficient Method Using Singularity Splines. NASA CR-2423, 1974.

8. Morino, L.; and Kuo, C. C.: Subsonic Potential Aerodynamics for Complex Configurations: A General Theory. AIAA J., vol. 12, no. 2, Feb. 1974, pp. 191-197.

9. Rubbert, P. E.; and Saaris, G. R.: Review and Evaluation of a Three Dimensional Lifting Potential Flow Analysis Method for Arbitrary Configurations. AIAA Paper 72-188, Jan. 1972.

10. Gloss, B. B.: Development of an Aerodynamic Theory Capable of Predicting Surface Loads on Slender Wings with Vortex Flow. Proceedings of the SCAR Conference, NASA CP-001, 1977. (Paper no. 3 of this compilation.)

11. Jones, R. T.; and Cohen, D.: High Speed Wing Theory. Princeton University Press, 1960, p. 158.

12. Carlson, H. W.: Aerodynamic Characteristics at Mach Number 2.05 of a Series of Highly Swept Arrow Wings Employing Various Degrees of Twist and Camber. NASA TM X-332, 1960.

13. Carlson, H. W.: Pressure Distributions at Mach Number 2.05 on a Series of Highly Swept Arrow Wings Employing Various Degrees of Twist and Camber. NASA TN D-1264, 1962.

14. D'Attorre, L.; Bilyk, M. A.; and Sergeant, R. J.: Three Dimensional Supersonic Flow Field Analysis of the B-1 Airplane by a Finite Difference Technique and Comparison with Experimental Data. AIAA Paper 74-189, 1974.

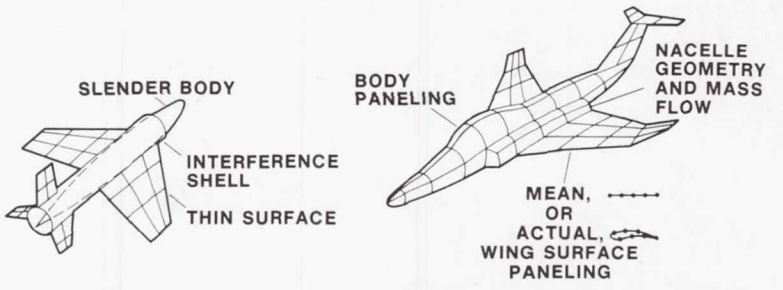

(a) INTERFERENCE SHELL MODEL (b) ARBITRARY SURFACE PANELING MODEL OF PRESENT METHOD

Figure 1.- Different levels of aerodynamic geometry modeling.

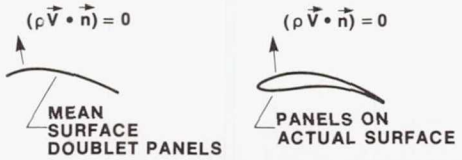

(a) VELOCITY OR MASS FLUX BOUNDARY CONDITIONS

(b) POTENTIAL TYPE BOUNDARY CONDITIONS FOR CLOSED BODIES (σ = SOURCE STRENGTH)

Figure 2.- Alternative forms for expressing boundary conditions.

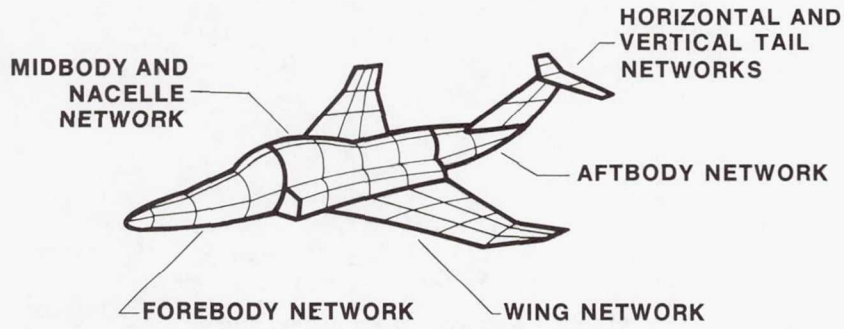

Figure 3.- Illustration of body surface broken into independently defined networks of panels.

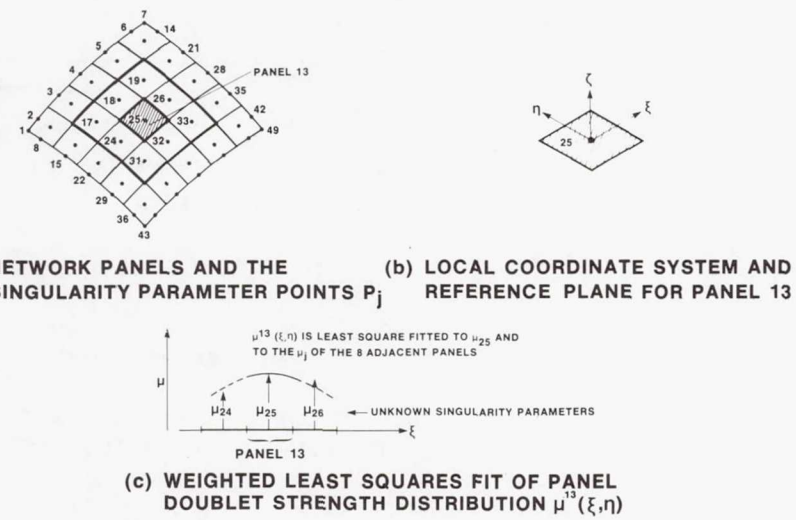

Figure 4.- Illustration of doublet/analysis network comprised of 25 panels and 49 singularity parameters.

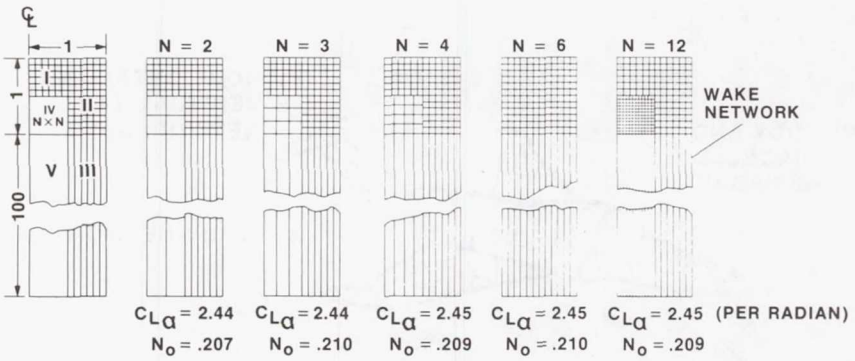

- **REGIONS I, II, III, IV, V ARE DISTINCT NETWORKS**
- **"EXACT SOLUTION OF $C_{L\alpha}$ = 2.47, N_o = 0.209 IS OBTAINED BY INCREASING PANEL DENSITY AT LEADING EDGE.**

Figure 5.- Localized changes in panel density; AR = 2, M = 0.

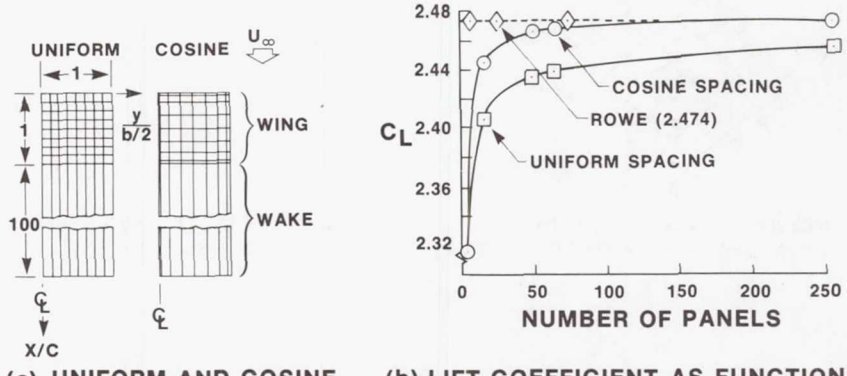

(a) UNIFORM AND COSINE PANEL SPACING

(b) LIFT COEFFICIENT AS FUNCTION OF NUMBER OF PANELS USED

Figure 6.- Convergence behavior of doublet/analysis panels; results scaled to α = 1 rad, M = 0. (The diamonds for the Rowe solution denote number of pressure modes, rather than number of panels.)

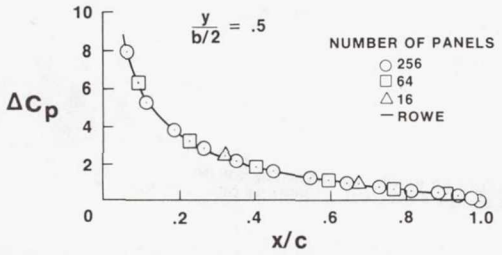

(c) CHORDWISE PRESSURE FOR COSINE SPACING

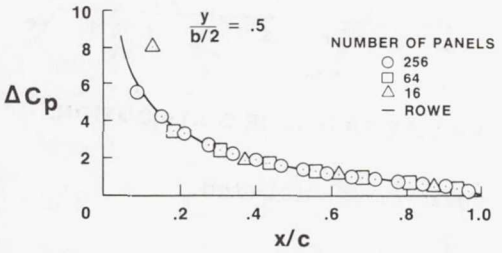

(d) CHORDWISE PRESSURE FOR UNIFORM SPACING

Figure 6.- Concluded.

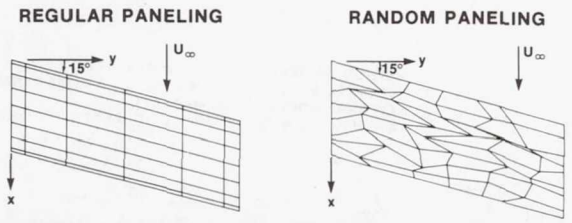

(a) MEAN SURFACE PANELING ARRANGEMENTS

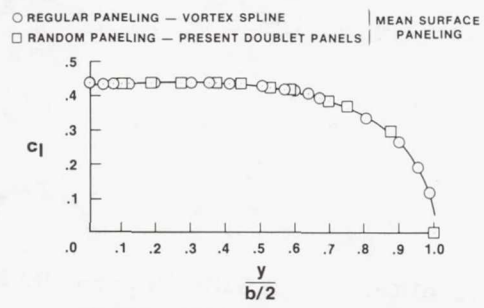

(b) SPANWISE LIFT DISTRIBUTION

Figure 7.- Insensitivity to panel arrangement;
$\alpha = 5.7^{o}$, $M = 0$.

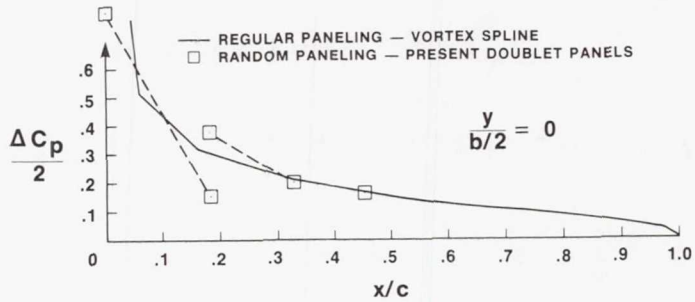

(c) CHORDWISE PRESSURE DISTRIBUTION;

Figure 7.- Concluded.

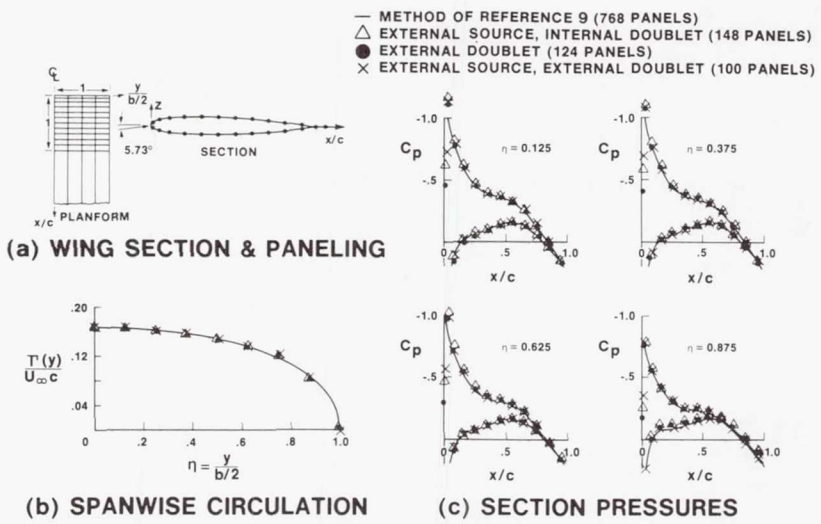

Figure 8.- Alternate surface paneling models.

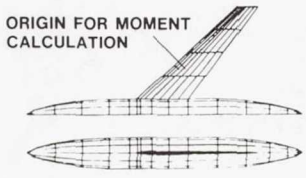

WING-BODY CONFIGURATION	PRESENT METHOD	METHOD OF REF. 9
SOURCE DISTRIB.	LINEAR	CONSTANT
PANEL GEOMETRY	CURVED	FLAT
NO. SOURCE PANELS	160	936
CPU TIME, sec.*	150	3300
C_L	.689	.697
C_m	.00345	−.00325

*CDC 6600

(a) SURFACE PANELING FOR PRESENT METHOD

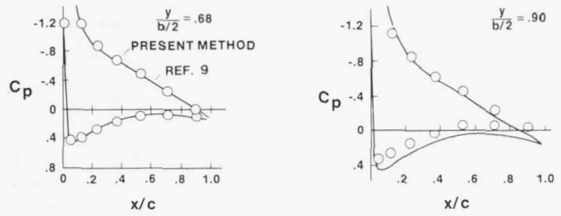

(b) CHORDWISE PRESSURE DISTRIBUTIONS

Figure 9.- Increased efficiency of current method over method using flat, constant strength sources; $\alpha = 10^{o}$, $M = 0$.

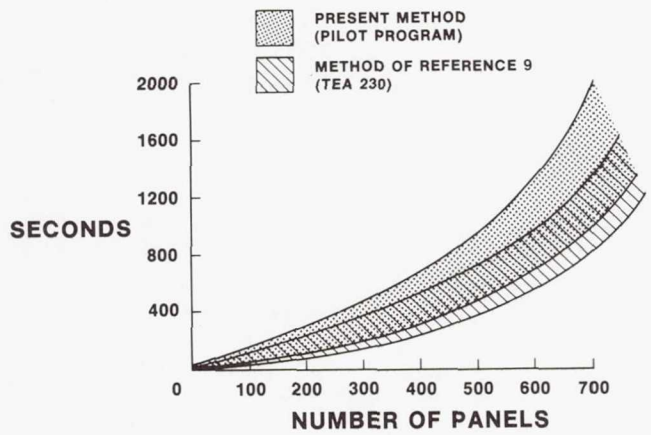

Figure 10.- Variation in CPU time with number of panels.

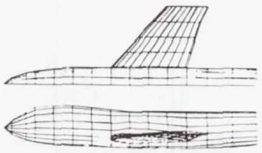

(a) PANELING OF DESIGN MODEL

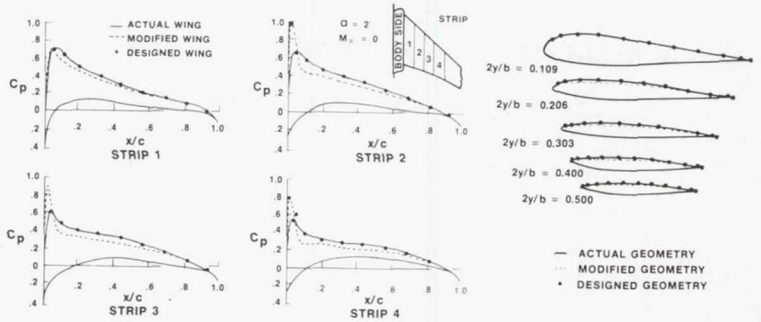

(b) WING-PRESSURE PROFILES — ANALYSIS MODE

(c) WING GEOMETRY

Figure 11.- Wing design in presence of fixed fuselage geometry.

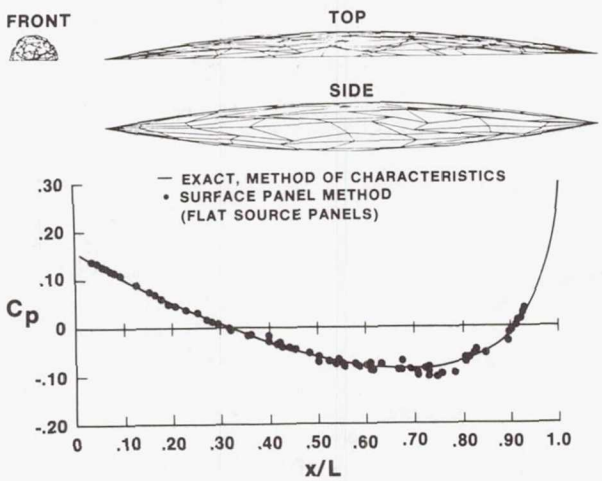

Figure 12.- Random source paneling on spindle, $\alpha = 0$; $M = \sqrt{2}$, fineness ratio = 0.1.

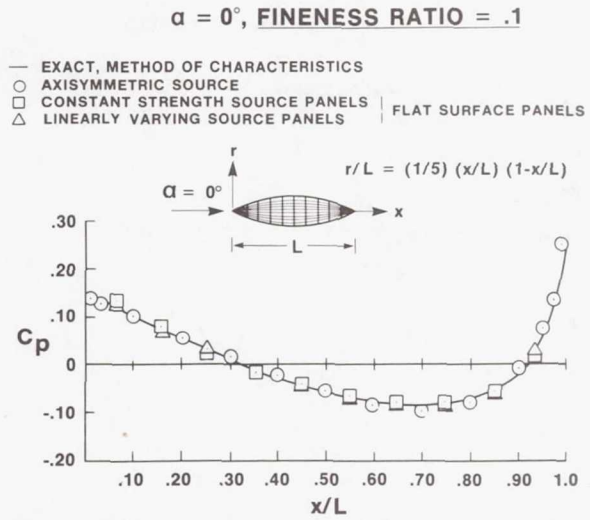

Figure 13.- Regular paneling for spindle of figure 12; M = $\sqrt{2}$.

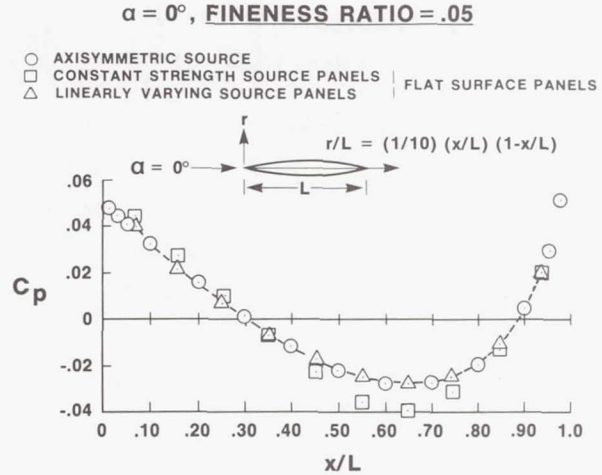

Figure 14.- Loss of accuracy for constant strength panel as fineness ratio is halved from that of figure 13; M = $\sqrt{2}$.

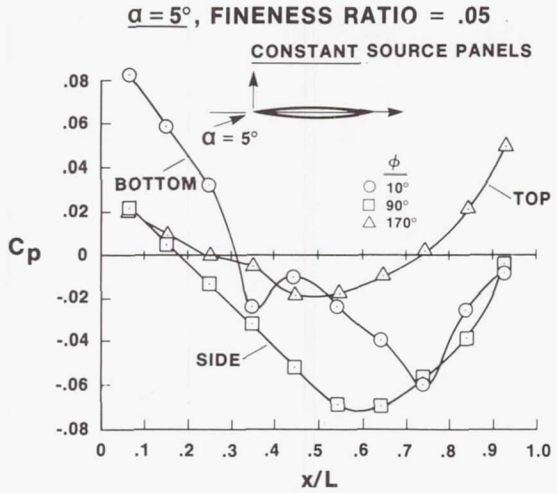

Figure 15.- Oscillatory solution produced by constant strength panels for spindle at angle of attack; $M = \sqrt{2}$.

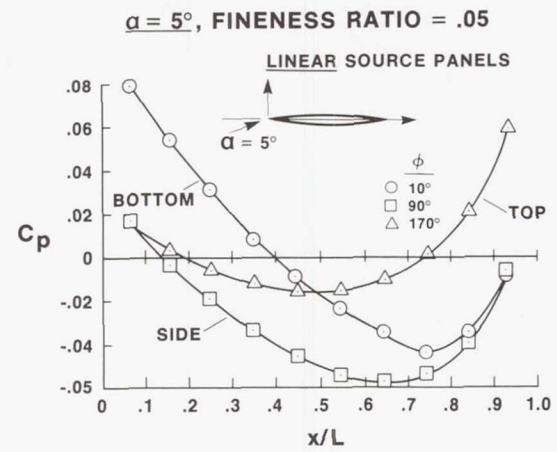

Figure 16.- Nonoscillatory solution produced by linear strength panels for configuration of figure 15; $M = \sqrt{2}$.

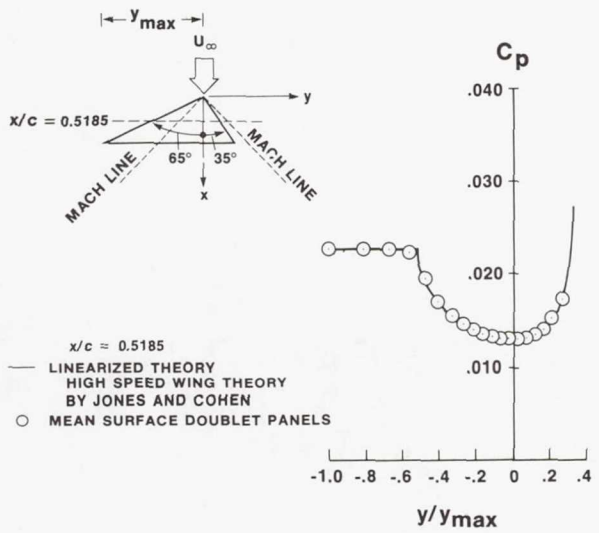

Figure 17.- Wing with subsonic and supersonic leading edges; $\alpha = 0.01$ rad, $M = \sqrt{2}$.

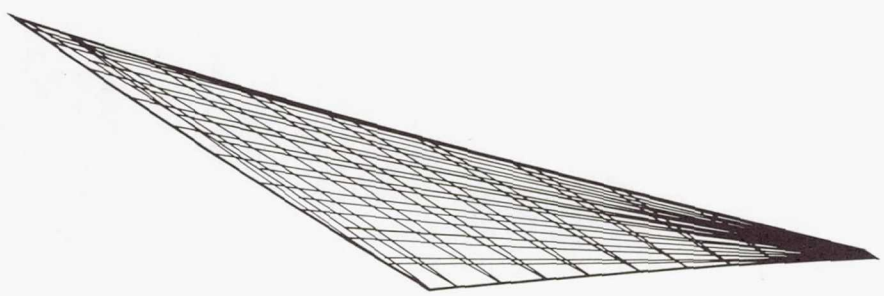

Figure 18.- Upper and lower surface paneling of 3% thick arrow wing.

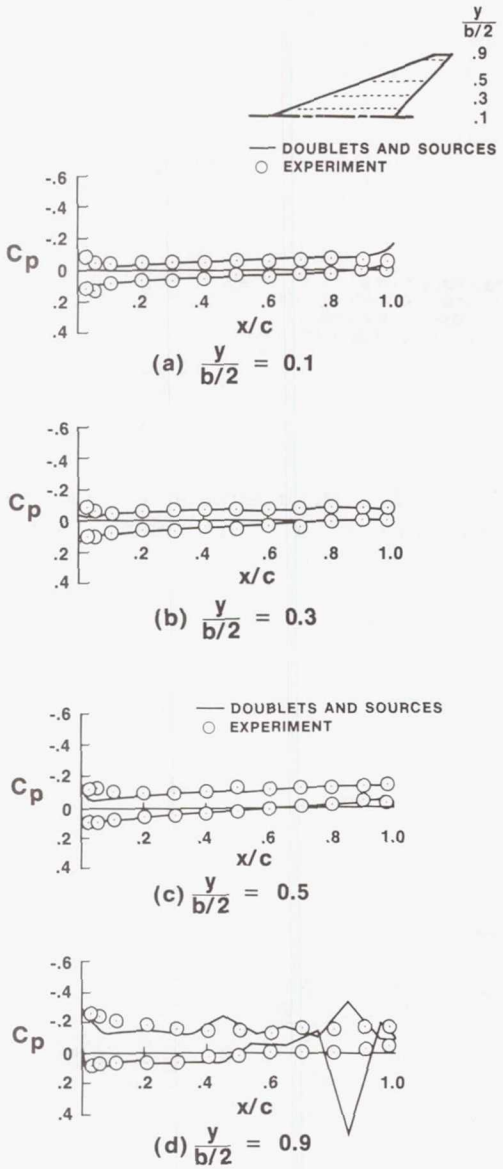

Figure 19.- Upper and lower surface pressures on 3% thick arrow wing; $\alpha = 2^{o}$, M = 2.05.

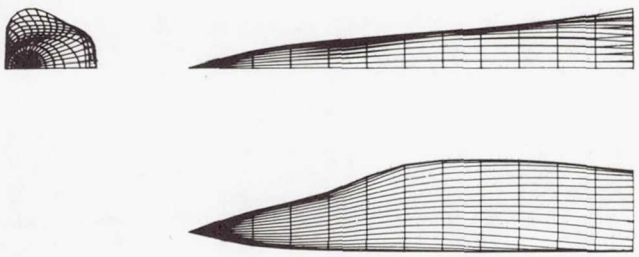

Figure 20.- Paneling on forebody of B-1 bomber.

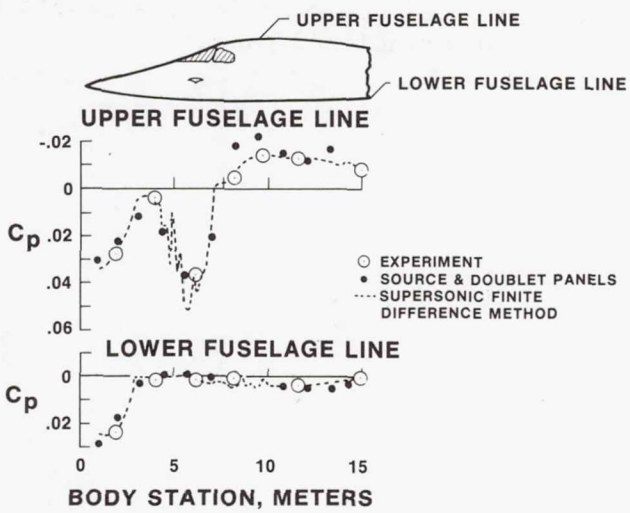

Figure 21.- Centerline pressures on forebody of B-1 bomber; $\alpha = 2^{o}$, $M = 1.6$.

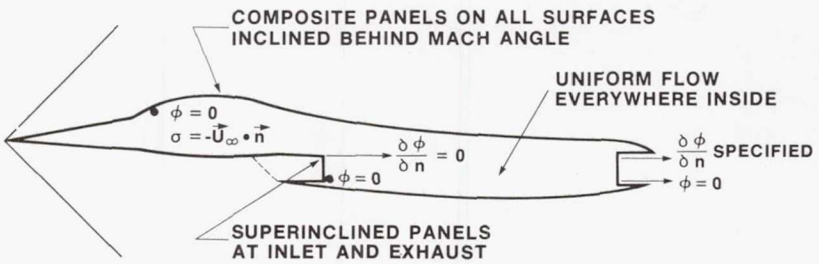

Figure 22.- Combined use of composite panels and superinclined panels.